Phase transition, elastic and electronic properties of topological insulator Sb_2Te_3 under pressure: First principle study*

Qing Lu(卢清)[1], Huai-Yong Zhang(张怀勇)[1], Yan Cheng(程艳)[1,2,†], Xiang-Rong Chen(陈向荣)[1,‡], and Guang-Fu Ji(姬广富)[3]

[1] *Institute of Atomic and Molecular Physics, College of Physical Science and Technology, Sichuan University, Chengdu* 610065, *China*

[2] *Key Laboratory of High Energy Density Physics and Technology of Ministry of Education, College of Physical Science and Technology, Sichuan University, Chengdu* 610064, *China*

[3] *National Key Laboratory of Shock Wave and Detonation Physics, Institute of Fluid Physics, Chinese Academy of Engineering Physics, Mianyang* 621900, *China*

(Received 28 June 2015; revised manuscript received 18 October 2015; published online 10 January 2016)

The phase transition, elastic and electronic properties of three phases (phase I, II, and III) of Sb_2Te_3 are investigated by using the generalized gradient approximation (GGA) with the PBESOL exchange–correlation functional in the framework of density-functional theory. Some basic physical parameters, such as lattice constants, bulk modulus, shear modulus, Young's modulus, Poisson's ratio, acoustic velocity, and Debye temperature Θ are calculated. The obtained lattice parameters under various pressures are consistent with experimental data. Phase transition pressures are 9.4 GPa (I→II) and 14.1 GPa (II→III), which are in agreement with the experimental results. According to calculated elastic constants, we also discuss the ductile or brittle characters and elastic anisotropies of three phases. Phases I and III are brittle, while phase II is ductile. Of the three phases, phase II has the most serious degree of elastic anisotropy and phase III has the slightest one. Finally, we investigate the partial densities of states (PDOSs) of three phases and find that the three phases possess some covalent features.

Keywords: Sb_2Te_3, phase transition, elastic properties, electronic properties

PACS: 64.60.–i, 62.20.D–, 71.20.–b **DOI:** 10.1088/1674-1056/25/2/026401

1. Introduction

Antimony telluride (Sb_2Te_3) is a member of the (Bi, $Sb)_2$(Te, $Se)_3$ family with a narrow band gap. These layered chalcogenides are typical thermoelectric materials.[1–3] Hence these materials and their alloys are widely studied. Compared with bulk Bi_2Te_3 alloy, the thin-film thermoelectric material demonstrates a significant enhancement in the figure of merit at 300 K.[4] First-principle calculations show that a uniaxial pressure applied perpendicularly to the plane of the layered structure substantially improves the power factor of Sb_2Te_3.[5] Calculations also show that under a uniaxial pressure of 1.5 GPa, multiple valence band maximal value occurs which may enhance thermoelectric properties.[6] Owing to the fast speed, excellent endurance, and low-programming energy, Sb_2Te_3 is a promising candidate for phase change random access memories (PRAMs).[7] Recently, chalcogenides (Sb_2Te_3, Bi_2Te_3, and Bi_2Se_3) have received attention again, because they are predicted to be three-dimensional (3D) topological insulators.[8–10] The topological insulator is a new class of material, which features single Dirac cone at the Γ point.[11]

Pressure can reduce interatomic distances and tune material properties, so high pressure study is helpful to understand properties of materials. Studies of these layered chalcogenides have shown that each of these chalcogenides presents a pressure-induced superconductivity.[12,13] Under ambient conditions, Sb_2Te_3 has a rhombohedral structure ($R\bar{3}m$, α-Sb_2Te_3, phase I).[14] It is a long puzzle to determine the crystalline structures of Sb_2Te_3 at high pressures.[15–17] Through the x-ray diffraction (XRD) experiments, Zhao *et al.*[18] reported that at about 9.3 GPa, Sb_2Te_3 started to transform from the rhombohedral structure to a monoclinic $C2/m$, and the transition to the monoclinic $C2/m$ structure was completed at 12.3 GPa. At about 15.1 GPa, another disordered monoclinic $C2/m$ structure emerged and this disordered $C2/m$ structure was completely formed at 18.9 GPa. Then, it transformed to a disordered body-centered cubic $Im\bar{3}m$ structure at about 19.8 GPa and this transformation was completed at above 29.7 GPa. Thus, Sb_2Te_3 underwent a sequence of phase transitions as follows: rhombohedral $R\bar{3}m$ structure → (9.3 GPa) monoclinic $C2/m$ structure → (15.1 GPa) disordered monoclinic $C2/m$ structure → (19.8 GPa) disordered body-centered

*Project supported by the National Natural Science Foundation of China (Grant Nos. 11204192 and 11174214) and Jointly supported by the National Natural Science Foundation of China and the China Academy of Engineering Physics (NSAF) (Grant No. U1430117).

†Corresponding author. E-mail: ycheng66@qq.com

‡Corresponding author. E-mail: xrchen66@qq.com

© 2016 Chinese Physical Society and IOP Publishing Ltd

cubic $Im\bar{3}m$ structure. In the following mentioned experiments, we just focus on the pressure under which the new phase emerges, but will not mention the pressure ranges of coexistence at all.

Using XRD experimental technique, Souza *et al.*[19] observed two high pressure phases at pressures of 9.8 GPa and 15.2 GPa, respectively. They determined that the first high pressure phase was of a monoclinic $C2/m$ structure and the second was of an ordered $C2/c$ structure. Recently, Ma *et al.*[20] also explored the high pressure behaviors of Sb_2Te_3 at pressures of up to 52.7 GPa through angle-dispersive synchrotron x-ray powder diffraction (XRPD) technique in a diamond anvil cell and their experimental results showed that the phase ($R\bar{3}m$, α-Sb_2Te_3) transformed into phase II (monoclinic sevenfold $C2/m$, β-Sb_2Te_3) and phase III (monoclinic eightfold $C2/c$, γ-Sb_2Te_3) around 8.0 GPa and 13.2 GPa, respectively, and at above 21.6 GPa, a disordered body-centered cubic $Im\bar{3}m$ structure (phase IV, δ-Sb_2Te_3) emerged. This phase sequence is consistent with the transition sequence of Bi_2Te_3.[21]

In our present work, using the plane-wave pseudopotential density functional theory (DFT) method as implemented in the Cambridge Serial Total Energy Package (CASTEP) code,[22,23] we investigate the phase transition and elastic properties of Sb_2Te_3 under pressure. Since the calculations of the disordered bcc phase are not possible in the CASTEP code, we just discuss the phases I, II, and III in our following calculations. The remaining parts of this paper are organized as follows. In Section 2, the computation details are presented. The results and discussion are shown in Section 3. Then electronic properties are discussed in Section 4. Finally, a summary of our results is given in Section 5.

2. Computation details

Equilibrium properties, such as bulk moduli, phonon frequencies and magnetisms are sensitive to lattice constants. Generally speaking, the lattice constants predicted from PBESOL[24,25] exchange–correlation functional were better than those predicted from the local spin density approximation (LSDA), the Perdew–Burke–Ernzerh (PBE) version of the generalized gradient approximation (GGA) or the Tao–Perdew–Staroverov–Scuseria (TPSS) meta-GGA. Thus the PBESOL was employed for describing the exchange–correlation energy of electrons. The ultrasoft "on the fly" pseudopotential[26] was chosen for the interaction of the electrons with the ion cores, and pseudo atomic calculations were performed for Sb-$5s^25p^3$ and Te-$5s^25p^4$. The electronic wave functions were expanded in a plane wave basis set with an energy cut-off of 260 eV. For the Brillouin-zone sampling, we used the Monkhorst–Pack meshs[27] $8\times8\times8$, $8\times8\times3$ and $3\times3\times2$ for phases I, II, and III, respectively. In the geometry optimization, criteria of convergence were set to be 5×10^{-6} eV/atom for energy, 0.01 eV/Å for force, 5×10^{-4} Å for ionic displacement, and 0.02 GPa for stress. In calculations of elastic properties, criteria of convergence were set to be 1×10^{-6} eV/atom for energy, 0.002 eV/Å for the maximum force, 1×10^{-4} for the maximum ionic displacement, and 0.003 GPa for the maximum strain amplitude. These parameters are carefully tested and sufficient to lead to a well converged total energy.

3. Results and discussion

3.1. Structural properties

The experimental atomic positions for all phases are presented as follows. The atomic positions of phase I are Sb occupied 6*c* Wyckoff site $(0,0,0.3988)$, Te_1 located at 3*a* Wyckoff site $(0,0,0)$, and Te_2 located at 6*c* Wyckoff site $(0,0,0.7872)$[14] under ambient conditions. At 13.2 GPa, the atomic positions of phase II are Sb_1 with 4*i* Wyckoff site $(0.1971,0,0.2079)$, Sb_2 with 4*i* Wyckoff site $(0.4599,0,0.2340)$, Te_1 with 4*i* Wyckoff site $(0.2321,0,0.3965)$, Te_2 with 4*i* Wyckoff site $(0.0451,0,0.6106)$, and Te_3 with 4*i* Wyckoff site $(0.3470,0,0.9853)$.[19] The atomic positions of phase III are Sb with 8*f* Wyckoff site $(0.278,0.1429,0.8396)$, Te_1 with 8*f* Wyckoff site $(0.5668,0.3853,0.9363)$, and Te_2 with 4*e* Wyckoff site (0.5,-0.0921,0.75)[20] at 20.5 GPa. These structures are also shown in Fig. 1. All calculations in our paper are rhombohedral representation for phase I and primitive cells for phase II and III. The geometry optimizations are performed for phases I, II, and III under pressure. The relaxed lattice parameters of unit cell of every structure at different pressures, together with calculated data cited from other papers and experimental results, are listed in Table 1. Obviously, our calculated lattice constants of phase I are in good agreement with the theoretical values.[17] After relaxing, the atomic positions of phase I are Sb wtih 6*c* Wyckoff site $(0,0,0.3988)$, Te_1 with at 3*a* Wyckoff site $(0,0,0)$, and Te_2 with 6*c* Wyckoff site $(0,0,0.7895)$ at 0 GPa. At 13.2 GPa, the relaxed atomic positions of phase II are Sb_1 with 4*i* Wyckoff site $(0.1726,0,0.1946)$, Sb_2 with 4*i* Wyckoff site $(0.4353,0,0.2135)$, Te_1 with 4*i* Wyckoff site $(0.2179,0,0.3924)$, Te_2 with 4*i* Wyckoff site $(0.0486,0,0.6208)$, and Te_3 with 4*i* Wyckoff site $(0.3696,0,1.0009)$. The relaxed atomic positions of phase III are Sb with 8*f* Wyckoff site $(0.2958,0.0981,0.8480)$, Te_1 with 8*f* Wyckoff site $(0.5975,0.3823,0.9530)$ and Te_2 with 4*e* Wyckoff site (0.5,-0.1137,0.75) at 20.5 GPa.

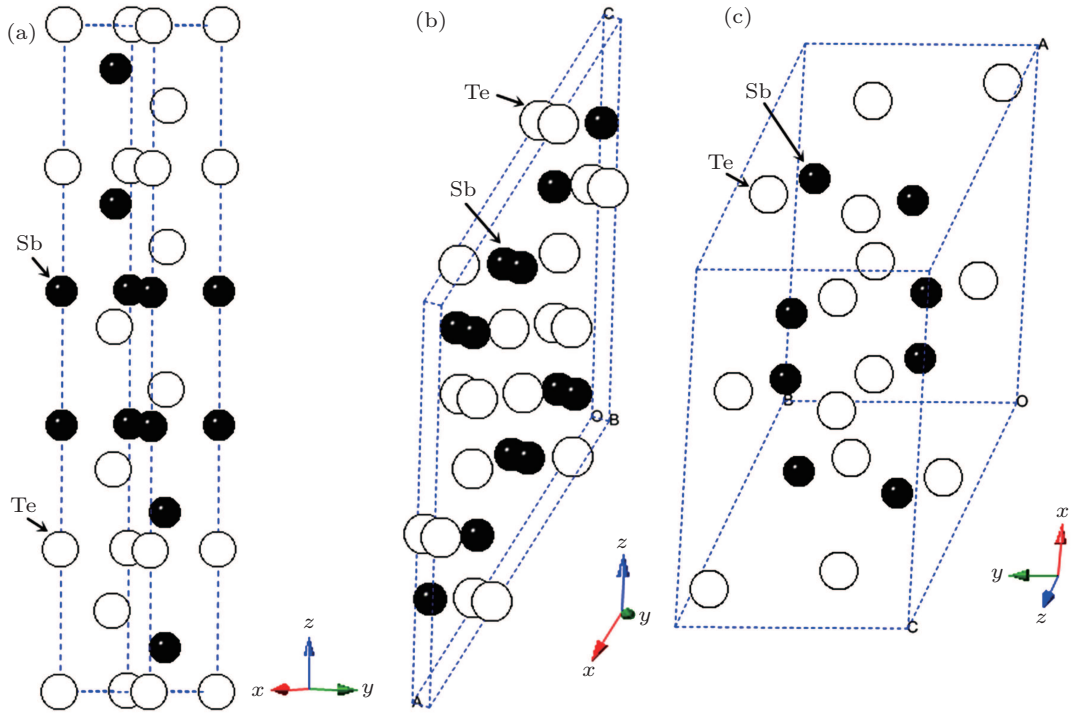


Fig. 1. (color online) Unit cells for (a) phase I at 0 GPa, (b) phase II at 13.2 GPa, and (c) phase III at 20.5 GPa. Phase I is the hexagonal representation.

Table 1. The relaxed lattice constants of unit cell of phases I, II, and III under different pressures, together with some experimental results and calculated data. Note that our results of hexagon or unit cells are transformed from the calculated data of rhombohedron or primitive cells.

	a/Å	b/Å	c/Å	β	Reference
α-Sb_2Te_3 (0 GPa)					
Th. (GGA-PBESOL)	4.272	4.272	29.737	120	this work
Th. (GGA-PBESOL)	4.276	4.276	29.940	120	[17]
Th. (GGA-PBE)	4.350	4.350	30.844	120	[5]
Exp.	4.264	4.264	30.458	120	[14]
Exp.	4.271	4.271	30.451	120	[19]
Exp.	4.265	4.265	30.450	120	[16]
β-Sb_2Te_3					
Th. (GGA-PBESOL) (10 GPa)	14.469	3.991	17.164	148.62	this work
Th. (GGA-PBESOL) (11.4 GPa)	14.415	3.965	17.052	148.56	this work
Th. (GGA-PBESOL) (13.2 GPa)	14.348	3.935	16.926	148.49	this work
Th. (GGA-PBE) (11.4 GPa)	14.573	4.082	17.241	149.15	[20]
Exp. (11.4 GPa)	14.449	4.063	17.519	149.64	[20]
Exp. (13.2 GPa)	14.372	4.014	17.090	149.12	[19]
γ-Sb_2Te_3					
Th. (GGA-PBESOL) (15 GPa)	9.632	6.769	10.208	134.51	this work
Th. (GGA-PBESOL) (20.5 GPa)	9.951	6.052	9.990	132.44	this work
Th. (GGA-PBE) (20.5 GPa)	9.676	6.850	10.103	135.36	[20]
Exp. (20.5 GPa)	9.706	6.704	10.055	135.56	[20]

The values of lattice constant a obtained from our calculations accord well with the experimental values[14,16,19] with the errors less than 0.2% and the errors of lattice constant c are about -2.4%. For comparison between the theoretical and experimental results, we present the lattice parameters of phase II at 11.4 GPa and 13.2 GPa and phase III at 20.5 GPa. All these calculated parameters are relatively consistent with the former experimental and theoretical results, which indicate that the selected exchange–correlation functional and pseudopotential are reasonable as well.

To investigate the phase transition of Sb_2Te_3, Gibbs free energy $G_{\text{Gibbs}} = E_{\text{internal}} + PV - TS$ will be used, where E_{internal}, P, V, T, and S are internal energy, pressure, volume, temperature, and vibrational entropy, respectively. At a given pressure P and temperature T, the thermodynamic stable phase has the lowest Gibbs free energy in candidates. In our

work, all the calculations are performed at zero K. Hence, the Gibbs free energy is equal to enthalpy $H = E_{\text{internal}} + PV$ and the transition pressure is the value which the crosspoint between enthalpies of two competitive structures corresponds to. To find out transition pressures from phase I to phases II and III, values of enthalpy of three structures are calculated under the pressures in a range of 0 GPa–28 GPa in steps of 4 GPa. Pressure dependences of enthalpy are plotted in Fig. 2. As the pressure increases, the enthalpy of each structure increases linearly. Thus we perform the linear fitting for enthalpy of each structure and obtain linear equations as follows:

$$\text{phase I}: \quad H = -3028.88621 + 0.81603P, \tag{1}$$

$$\text{phase II}: \quad H = -3028.58411 + 0.78378P, \tag{2}$$

$$\text{phase III}: \quad H = -3028.11888 + 0.75071P. \tag{3}$$

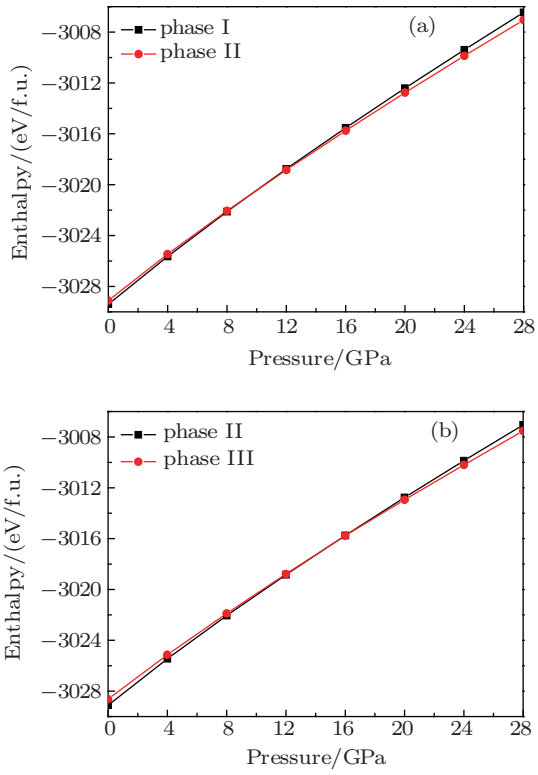


Fig. 2. (color online) Variations of enthalpy with pressure (a) for phase I to phase II, (b) for phase II to III.

Solving Eqs. (1) and (2), we obtain that the transition pressure from phase I to phase II is 9.4 GPa, which accords with experimental values 9.3 GPa,[18] 9.8 GPa[19] and 8 GPa.[20] Similarly, according to Eqs. (2) and (3), we find that the change from phase II to phase III occurs at about 14.1 GPa, which is also consistent with experimental results 14.5 GPa,[17] 15.2 GPa[19] and 13.2 GPa.[20] Moreover, the variations of volume per formula unit for the three phases are shown in Fig. 3. The volume of each phase decreases with increasing pressure. When the phase transition occurs, we can measure the relative volume collapse by using $\Delta V_P/V_0$, where V_0 is the ground state volume per formula unit. From phase I to phase II, $\Delta V_{P1}/V_0$ is about 3.6%, and $\Delta V_{P2}/V_0$ is about 2.6% from phase II to phase III.

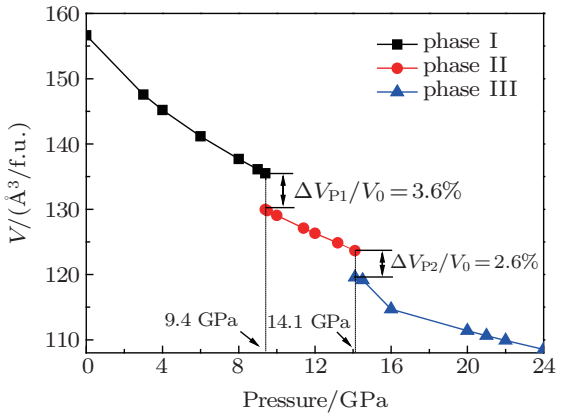


Fig. 3. (color online) Variations of volume per formula unit with pressure for three phases.

3.2. Elastic properties

Elastic constant that relates stress to strain is of great importance for a material and helpful for understanding the acoustic velocity, bulk modulus and shear modulus. Therefore, we investigate the elastic constants of all three phases (0 GPa for phase I, 10 GPa for phase II and 15 GPa for phase III). As shown in Table 2, there are six independent elastic constants in the rhombohedral structure and the monoclinic phases have thirteen independent elastic constants.

Table 2. Calculated elastic constants C_{ij} (GPa) of Sb_2Te_3 with phase I at 0 GPa, phase II at 10 GPa, and phase III at 15 GPa.

	C_{11}	C_{22}	C_{33}	C_{44}	C_{55}	C_{66}	C_{12}	C_{13}	C_{14}	C_{15}	C_{23}	C_{25}	C_{35}	C_{46}
I	85.5		50.5	37.9			21.0	30.8	–21.1					
II	149.6	146.6	157.2	30.0	22.4	98.5	112.8	48.5		–3.6	29.7	–13.5	2.0	–14.5
III	218.7	159.8	245.3	70.3	92.6	125.2	98.7	83.3		–22.6	62.7	–18.0	28.9	–31.9

From the calculated elastic constants, we can obtain the Voigt average for bulk modulus (B_V) and shear modulus (G_V), together with the Reuss average for bulk modulus (B_R) and shear modulus (G_R).[28,29] According to the Voigt–Reuss–Hill approximations,[30] the bulk modulus B and shear modulus G are defined as the arithmetic average of Reuss and Voight values: $B = (B_R + B_V)/2$, $G = (G_R + G_V)/2$. As shown in Table 3, at the ground state, the bulk modulus B of phase I

is 42.1 GPa and in agreement with the experimental result 36.1 GPa[19] and theoretical value 41.0 GPa.[17] The bulk modulus B of phase II is 90.5 GPa at 10 GPa and 0 K and that of phase III is 121.3 GPa at 15 GPa and 0 K. From phase I to phase III, the value of B increases, implying that Sb_2Te_3 is more and more difficult to compress. Obviously, for each structure, its value of G (see Table 3) is smaller than B, which indicates that a shear deformation occurs more easily and shear modulus G is the parameter limiting the stability of Sb_2Te_3. The value of G of phase I is smaller than other phases, suggesting that the shear deformation is easier to occur in phase I. The shear modulus G is also an important parameter related to the hardness of a crystal. The value of G increases from phase I to phase III, indicating that the hardness of Sb_2Te_3 may increase under pressure. The brittleness or ductility has an important influence on applications of a material and there is an empirical criterion as follows: if $B/G < 1.75$, the material behaves as a brittle manner, otherwise, it behaves as a ductile manner.[31] The values of B/G of phase I (1.67) and phase III (1.61) are less than the critical value 1.75, while the value of B/G for phase II (2.37) is larger than 1.75, which means that phases I and III are brittle, while phase II is ductile.

Table 3. Calculated values of bulk modulus B (GPa), shear modulus G (GPa) and B/G.

	P/GPa	B_V/GPa	B_R/GPa	B/GPa	G_V/GPa	G_R/GPa	G/GPa	B/G
I	0	42.9	41.3	42.1	30.9	19.7	25.3	1.67
II	10	92.8	88.2	90.5	47.7	28.8	38.2	2.37
III	15	123.7	118.9	121.3	82.9	67.5	75.2	1.61

Young's modulus E can measure stiffness of solid. The larger the value of E, the stiffer the material is. Poisson's ratio σ gives information about the feature of bonding forces and Debye temperature Θ is a useful parameter and related to many physical properties, such as specific heat and melting temperature. Also it is usually believed that the quantum effect of material is remarkable below Debye temperature Θ, while it can be ignored above Debye temperature Θ. The Young's modulus E, Poisson's ratio σ, and Debye temperature Θ can be obtained from[32]

$$E = \frac{9BG}{3B+G}, \quad \sigma = \frac{1}{2}\left(\frac{3B-2G}{3B+G}\right),$$
$$\Theta = \frac{h}{k}\left[\frac{3n}{4\pi}\left(\frac{N_A\rho}{M}\right)\right]^{1/3} V_m, \tag{4}$$

where h is the Planck's constant, k is the Boltzmann's constant, N_A is the Avogadro's number, n is the number of atoms per formula unit, M is the molecular mass per formula unit, ρ is the density, and V_m is average acoustic velocity and can be calculated from

$$V_m = \left[\frac{1}{3}\left(\frac{2}{V_S^3} + \frac{1}{V_L^3}\right)\right]^{-1/3},$$

$$V_S = \sqrt{\frac{G}{\rho}}, \quad V_L = \sqrt{\frac{B+(4/3)G}{\rho}}, \tag{5}$$

where V_S and V_L are the shear and longitudinal acoustic velocity, respectively. The values of E, σ, Θ, V_S, V_L, and V_m are listed in Table 4. Obviously, the value of E increases gradually from phase I to phase III. This means that the stiffness is enhanced, as the pressure rises. If the value of σ is in a range of $0.25-0.5$,[33] interatomic forces will be central. Thus phase I ($\sigma = 0.2499$) and phase III ($\sigma = 0.2431$) are noncentral force solids, while phase II ($\sigma = 0.3148$) is a central force solid. In addition, the values of V_S are 1.95 km/s, 2.18 km/s, 2.93 km/s, respectively for phases I, II, and III . As for V_L, they are 3.38 km/s, 4.19 km/s, 5.03 km/s, respectively. It is found that the values of V_S and V_L increase gradually from phase I to phase III, so the V_m increases (see Table 4). Using these data, we can obtain the Debye temperature Θ and it has the same increasing tendencies for phases I–III. At 80 K, the Debye temperature Θ is 160 K[34] and a little smaller than our calculated result of 205 K. The values of Debye temperature Θ of phases II and III are 246 K and 337 K, respectively. However, there are no values of experimental Debye temperature Θ for phases II and III to be compared with each other.

Table 4. Values of longitudinal acoustic velocity V_L (km/s), shear acoustic velocity V_S (km/s), average acoustic velocity V_m (km/s), Debye temperature Θ (K), Young's modulus E (GPa), Poisson's ratio σ, and universal elastic anisotropy index A^u of Sb_2Te_3.

Sb_2Te_3	P/GPa	V_S/(km/s)	V_L/(km/s)	V_m/(km/s)	Θ/K	E/GPa	σ	A^u
I	0	1.95	3.38	2.17	205	63.2	0.2499	2.9
II	10	2.18	4.19	2.44	246	100.6	0.3148	3.3
III	15	2.93	5.03	3.25	337	187.0	0.2431	1.2

Practically all elastic single crystals are anisotropic to a certain degree. Hence A^{u}, a universal anisotropy index,[35,36] is employed to estimate the elastic anisotropy of Sb_2Te_3 and expressed as

$$A^{\mathrm{u}} = 5\frac{G_V}{G_R} + \frac{B_V}{B_R} - 6 \geq 0. \quad (6)$$

The deviation of A^{u} from zero indicates the extent of single crystal anisotropy and accounts for both the shear and the bulk contributions. As for Sb_2Te_3, the order of A^{u} values is phase II (3.3) > phase I (2.9) > phase III (1.2), implying that of the three phases, phase II has the most serious degree of elastic anisotropy and phase III has the slightest one.

4. Electronic properties

The partial densities of states (PDOSs) of three phases, i.e., phase I at 0 GPa, phase II at 10 GPa and phase III at 15 GPa are shown in Fig. 4. For phase I (see Fig. 4(a)), the lower valence band (−14 eV–10.5 eV) is contributed from Sb-5s, Sb-5p, Te_1-5s, and Te_2-5s states. The middle valence band (−10 eV ∼ −7 eV) originates from Sb-5s, Te_1-5s, Te_2-5s, Te_1-5p, and Te_2-5p states in which the Sb-5s states are dominant. The upper valence band (−6 eV ∼ 0 eV) is mainly comprised of the contributions from Sb-5s, Sb-5p, Te_1-5p, and Te_2-5p states, and it is dominated by Sb-5p, Te_1-5p, and Te_2-5p states. In the conduction band, the Sb-5p, Te_1-5p, and Te_2-5p states play the dominant role in a range from 0 eV to 5 eV and the range from 5 eV to 9 eV consists of the constructions from Sb-5s, Te_1-5s, and Te_2-5s states. According to the analysis above, in the whole valence band, we discover that Sb-5s states hybridize with Te-5s states in an energy range from −14 eV to −7 eV and Sb-5p states strongly hybridize with Te-5p states from −6 eV to 0 eV. These hybridizations imply the existence of covalent bonding in α-Sb_2Te_3. For phase II (Fig. 4(b)), in the valence band, the energy range from −15 eV to −7 eV is mainly composed of the contributions from Sb_1-5s, Sb_2-5s, Te_1-5s, Te_2-5s, and Te_3-5s states. The Sb_1-5p, Sb_2-5p, Te_1-5p, Te_2-5p, and Te_3-5p states play a dominant role in an energy range from −7 eV to 5 eV. For phase III (Fig. 4(c)), Sb-5s, Te_1-5s, and Te_2-5s states contribute to the energy range from −15.5 eV to −7.5 eV. The energy range from −7 eV to 5 eV is dominated by Sb-5p, Te_1-5p, and Te_2-5p states. From the analysis, we can notice that the hybridization between Sb-5s and Te-5s states and hybridization between Sb-5p and Te-5p states also exist in phases II and phase III. These hybridizations also indicate that there exist the covalent bondings in β-Sb_2Te_3 and γ-Sb_2Te_3. It is found that energy range of conduction band of each of phases II and III is smaller than that of phase I, while energy ranges of valence band of phases II and III are slightly larger than that of phase I. Furthermore, the pressure-induced metallization is a well-known phenomenon in semiconductor. From the PDOSs of high pressure phases, we can infer that they exhibit a metallic behavior, which accords with the conclusion of other paper.[20]

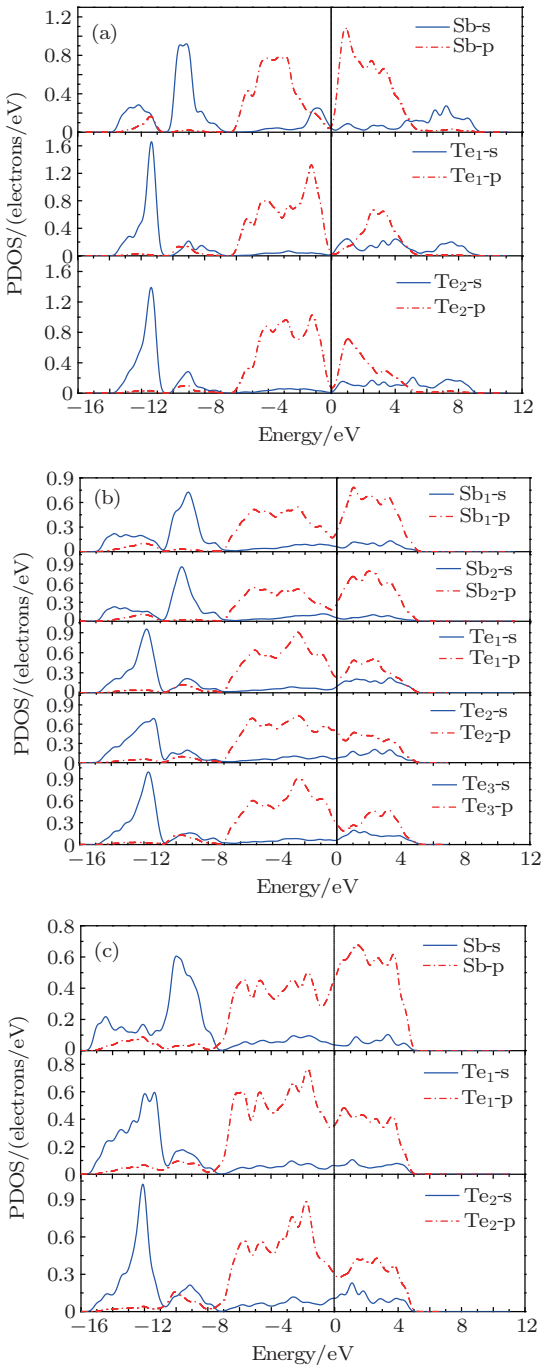


Fig. 4. (color online) Calculated PDOS versus energy for (a) phase I at 0 GPa, (b) phase II at 10 GPa, and (c) phase III at 15 GPa.

5. Conclusions

In this work, we study the phase transitions, elastic and electronic properties of α-Sb_2Te_3 ($R\bar{3}m$), β-Sb_2Te_3 ($C2/m$) and γ-Sb_2Te_3 ($C2/c$), by using first principle calculations

based on the density functional theory. The calculated lattice constants of three phases are in agreement with their experimental values. The enthalpies of all the structures are calculated under a pressure range of 0 GPa–28 GPa. Solving the cross-point of enthalpy, we obtain the phase transition pressures to be 9.4 GPa for phases I to II and 14.1 GPa for phase II to phase III respectively. These results are consistent with experimental data. Elastic constants C_{ij}, bulk modulus B, shear modulus G of the three phases are calculated and the obtained values of B/G indicate that phase I and III are brittle, while the phase II is ductile. Young's modulus E, Poisson's ratio σ, shear acoustic velocity $V_{\rm S}$, longitudinal acoustic velocity $V_{\rm L}$, average acoustic velocity $V_{\rm m}$, and Debye temperature Θ are also studied and all these quantities increase from phase I to phase III, except the Poisson's ratio σ. The universal anisotropy index $A^{\rm u}$ suggests the order of degree of elastic anisotropy is phase II (3.3) $>$ phase I (2.9) $>$ phase III (1.2). In the end, the partial densities of states are studied, suggesting that there are some covalent features in the three phases and high pressure phases show metallic behaviors.

References

[1] Snyder G J and Tobere E S 2008 *Nat. Mater.* **7** 105
[2] Cao Y Q, Zhao X B, Zhu T J, Zhang X B and Tu J P 2008 *Appl. Phys. Lett.* **92** 143106
[3] Kadel K, Kumari L, Li W Z, Huang J Y and Provencio P P 2011 *Nanoscale Res. Lett.* **6** 57
[4] Venkatasubramanian R, Siivola E, Colpitts T and O'Quinn B 2001 *Nature* **413** 597
[5] Thonhauser T, Scheidemantel T J, Sofo J O, Badding J V and Mahan G D 2003 *Phys. Rev. B* **68** 085201
[6] Larson P 2006 *Phys. Rev. B* **74** 205113
[7] Yin Y, Sone H and Hosaka S 2007 *J. Appl. Phys.* **102** 064503
[8] Zhang H, Liu C X, Qi X L, Dai X, Fang Z and Zhang S C 2009 *Nat. Phys.* **5** 438
[9] Chen Y L, Analytis J G, Chu J H, Liu Z K, Mo S K, Qi X L, Zhang H J, Lu D H, Dai X, Fang Z, Zhang S C, Fisher I R, Hussain Z and Shen Z X 2009 *Science* **325** 178
[10] Zhang W, Yu R, Zhang H J, Dai X and Fang Z 2010 *New J. Phys.* **12** 065013
[11] Zhang T, Cheng P, Chen X, Jia J F, Ma X, He K, Wang L, Zhang H, Dai X, Fang Z, Xie X and Xue Q K 2009 *Phys. Rev. Lett.* **103** 266803
[12] Einaga M, Tanabe Y, Nakayama A, Ohmura A, Ishikawa F and Yamada Y 2010 *J. Phys. Conf. Ser.* **215** 012036
[13] Zhang J L, Zhang S J, Weng H M, Zhang W, Yang L X, Liu Q Q, Feng S M, Wang X C, Yu R C, Cao L Z, Wang L, Yang W G, Liu H Z, Zhao W Y, Zhang S C, Dai X, Fang Z and Jin C Q 2011 *Proc. Natl. Acad. Sci. USA* **108** 24
[14] Anderson T L and Krause H B 1974 *Acta Cryst. B* **30** 1307
[15] Sakai N, Kajiwara T, Takemura K, Minomura S and Fujii Y 1981 *Solid State Commun.* **40** 1045
[16] Jacobsen M K, Kumar R S, Cornelius A L, Sinogeiken S V and Nicol M F 2007 *AIP Conf. Proc.* **955** 171
[17] Gomis O, Vilaplana R, Manjón F J, Rodríguez-Hernández P, Pérez-González E, Muñoz A, Kucek V and Drasar C 2011 *Phys. Rev. B* **84** 174305
[18] Zhao J, Liu H, Ehm L, Chen Z, Sinogeikin S, Zhao Y and Gu G 2011 *Inorg. Chem.* **50** 11291
[19] Souza S M, Poffo C M, Trichês D M, Lima J C, Grandi T A, Polian A and Gauthier M 2012 *Physica B* **407** 3781
[20] Ma Y, Liu G, Zhu P, Wang H, Wang X, Cui Q, Liu J and Ma Y 2012 *J. Phys.: Condens. Matter* **24** 475403
[21] Zhu L, Wang H, Wang Y, Lv J, Ma Y, Cui Q, Ma Y and Zou G 2011 *Phys. Rev. Lett.* **106** 145501
[22] Payne M C, Teter M P, Allen D C, Arias T A and Joannopoulos J D 1992 *Rev. Mod. Phys.* **64** 1045
[23] Milman V, Winkler B, White J A, Packard C J, Payne M C, Akhmatskaya E V and Nobes R H 2000 *Int. J. Quantum Chem.* **77** 895.
[24] Perdew J P, Ruzsinszky A, Csonka G I, Vydrov O A, Scuseria G E, Constantin L A, Zhou X and Burke K 2008 *Phys. Rev. Lett.* **100** 136406
[25] Perdew J P, Ruzsinszky A, Csonka G I, Vydrov O A and Scuseria G E 2008 *Phys. Rev. Lett.* **101** 239702
[26] Vanderbilt D 1990 *Phys. Rev. B* **41** 7892
[27] Monkhorst H J and Pack J D 1976 *Phys. Rev. B* **13** 5188
[28] Berryman J G and Mech J 2005 *Phys. Solids* **53** 2141
[29] Wu Z, Zhao E, Xiang H, Hao X, Liu X and Meng J 2007 *Phys. Rev. B* **76** 054115
[30] Hill R 1952 *Proc. Soc. London A* **65** 349
[31] Pugh S F 1954 *Philos. Mag.* **45** 823
[32] Cheng C, Lv Z L, Cheng Y and Ji G F 2014 *J. Alloys Compd.* **603** 183
[33] Chu F, He Y, Thoma D J and Mitchell T E 1995 *Scr. Metal. Mater.* **33** 1295
[34] Dyck J S, Chen W, Uher C, Drašar Č and Lošt'ák P 2002 *Phys. Rev. B* **66** 125206
[35] Ranganathan S I and Ostoja-Starzewski M 2008 *Phys. Rev. Lett.* **101** 055504
[36] Ding A L, Li C M, Wang J, Ao J, Li F, and Chen Z Q 2014 *Chin. Phys. B* **23** 096201